Turkish Journal of Electrical Engineering & Computer Sciences

http://journals.tubitak.gov.tr/elektrik/

Research Article

Turk J Elec Eng & Comp Sci
(2015) 23: 1698 – 1714

doi:10.3906/elk-1404-236

Low-cost sliding mode control of WECS based on DFIG with stability analysis

Abdelhak DJOUDI[1,2,*], **Hachemi CHEKIREB**[2], **El Madjid BERKOUK**[2], **Seddik BACHA**[3]

[1]Renewable Energy Development Center (CDER), Algiers, Algeria
[2]National Polytechnic School, Process Control Laboratory (LCP), El-Harrach, Algiers, Algeria
[3]Grenoble Alpes University, G2Elab, Grenoble, France

Received: 13.04.2014 • **Accepted/Published Online:** 05.03.2015 • **Printed:** 30.11.2015

Abstract: The aim of this work is to developing sliding mode control of active and reactive stator powers produced by a wind energy conversion system (WECS), based on doubly fed induction generator (DFIG). A flux estimation model and rotor current sensor are no longer required. The controller is developed from the DFIG nonlinear-coupled model. Moreover, the global stability and the DFIG states' boundedness when our low-cost sliding mode control is applied are established analytically. It is revealed that the (dq) components of the rotor flux remain near their nominal values. Our approach is validated via simulation in the case of a WECS based on DFIG rating at 1.5 MW. The robustness and the performances are verified with the presence of parametric variations and disturbances in the case of an unbalanced grid.

Key words: Doubly fed induction generator, robustness and stability, sliding mode control, rotor current sensorless, wind energy conversion system

1. Introduction

During the past years, more attention and interest have been paid to wind energy utilization due to its economic and environment advantages. Indeed, by the end of 2011, 238.5 GW of wind turbine capacity was installed across the world [1]. Nowadays, many wind farms are based on doubly fed induction generator (DFIG) technology due to its advantages compared to others generators, where the dimension of the electronic power converter is reduced to about 25% to 30% of the generator rating, which leads to lower converter costs and power losses [2].

Several research works have been undertaken to enhance the operation efficiency of wind energy conversion systems (WECSs) [2–19]. It is well established that a DFIG-based WECS, acting under variable speed, allows extraction of the maximum available wind power [5–7]. For this goal, various methods have been presented in the literature. Among them, we highlight the direct control of the rotor current scheme [8], direct torque control [9,10], torque and reactive stator power control [11,12], active and reactive stator power control [2–4,13–18], and speed control [19]. To overcome the drawbacks of this last one, the speed and reactive stator power or flux control can be also considered. Practice in this field has shown that stator power control is more efficient because it allows us to directly impose the power factor and to easily limit the active power transient from the WECS in the case of overpowering.

The vector control (VC) method is the classical stator power control of a WECS based on a DFIG. This control scheme is generally derived from a simplified and decoupled DFIG model [3,4,13,14,18] where

*Correspondence: ab.djoudi@cder.dz

some existing interactions are simply ignored. This VC control exhibits low performances and low robustness compared to those of control methods based on the DFIG nonlinear model.

For this, two main methods have been proposed. One is based on the optimal switching table of the switches' states related to the rotor side converter where the control errors of the stator powers are minimized using the DFIG electrical states [2,16,17]. This method is valid only in the case of the conventional DC/AC converter and requires complicated online calculations, and it displays oscillations when the generator operates near its synchronous speed [15]. The second method concerns sliding mode control (SMC) [15]. In this work, the controller is derived in the stator reference frame. This latter one is independent of the angular position of the vector, related to some electrical quantities, which is essential when a synchronous coordinate transformation is used.

The classical method applied to estimate the stator or rotor flux, incorporating an integral function, displays high sensibility to stator or rotor resistance variations. Therefore, the estimated flux can deviate greatly from its real value. All control methods mentioned above require rotor current sensors.

In order to avoid the problem caused by the classical method of flux estimation, eliminating the rotor current sensors and keeping the same performances and robustness as in [15], we intend in our work to elaborate on the SMC of the stator powers based on a nonlinear state space model of a DFIG. The state vector contains the stator powers, the rotor flux, and rotor speed pulsation. The control law is computed using the nominal dq flux components instead of real ones. Notice that in our approach, a rotor flux estimation model is not used.

It is also worth noticing that the problems related to the global stability of the control and the boundedness of DFIG states are not treated in the majority of papers, including [2–4,8–19]. In order to highlight the viability of the proposed approach, the global stability and the boundedness of the DFIG electrical states are established.

The paper is organized as follows: in Section 2, the considered WECS is described concisely and some important details about its operation are given. Moreover, the state model of the DFIG is presented, from which the dynamics of the output are derived. This model allows us to determine the nominal rotor flux components. Section 3 is devoted to the SMC of the stator powers, where the ideal control law and the proposed control based on the nominal rotor flux components are developed. In this same section, the stability and robustness of the proposed control law are studied. Discussion of the states' boundedness and trajectories when this plant is driven by the proposed SMC is carried out in Section 4. The simulation results and their analysis, related to the considered WECS based on a DFIG of 1.5 MW power rating, are given in Section 5.

2. The considered WECS

2.1. Preliminary considerations

The scheme of the used WECS-based DFIG is given in Figure 1, where the stator is directly connected to the grid and the rotor windings are also coupled to the network through an AC/AC converter. Under the effect of the wind, the turbine produces a torque τ_w on its shaft that rotates at speed ω_w. Due to the effect of the multiplier, with coefficient m_c, the speed related to the shaft generator ω_G is augmented and the torque of the shaft generator τ_G is reduced such that:

$$\omega_G = m_c \omega_w; \quad \tau_G = \tau_w / m_c. \tag{1}$$

Torque τ_w and mechanical power P_w extracted from the wind can be calculated as follows:

$$\tau_w = P_w / \omega_w, \tag{2}$$

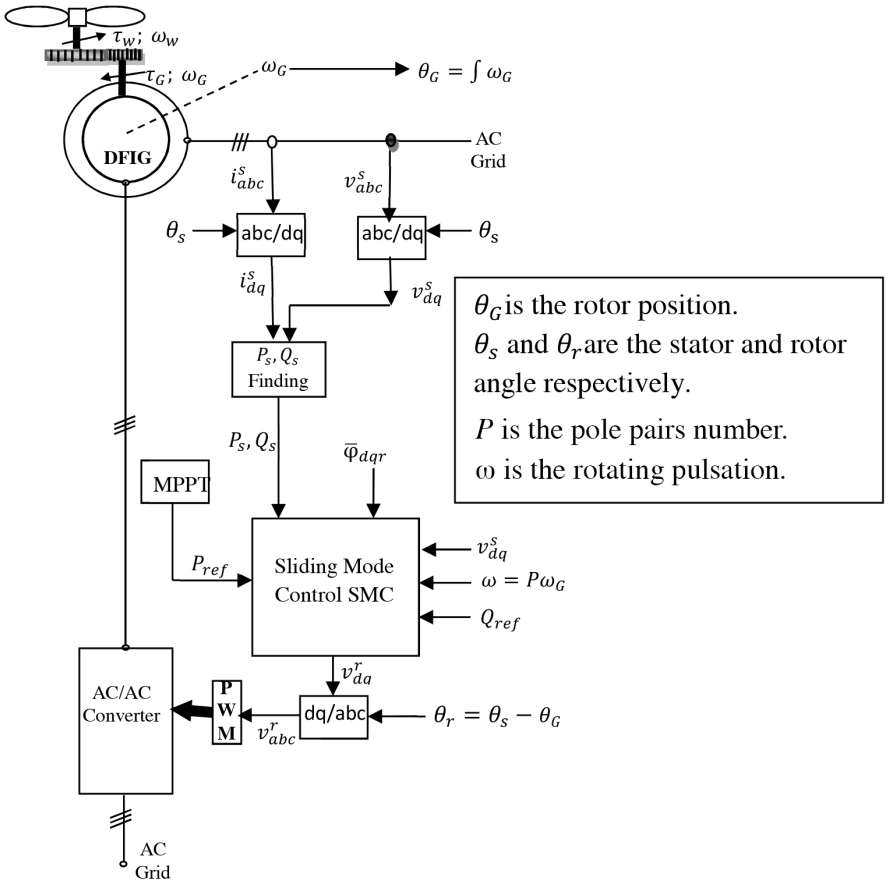

Figure 1. Scheme of the considered wind turbine system.

$$P_w = \frac{1}{2}\pi\rho C_p\left(\beta,\lambda\right)R^2V_w^3; \quad \lambda = R\omega_w/V_w, \tag{3}$$

where ρ, R, and λ are respectively the air density, the wind turbine radius, and the ratio of the blade tip speed to wind speed V_w. Moreover, the coefficient C_p is related to the characteristic of the wind turbine and it depends on the ratio λ and the inclination of the blades β.

The maximum power point tracking (MPPT) algorithm is exploited to detect the active stator power reference P_{ref} necessary to maintain the coefficient C_p at its maximal value in order to extract the maximum power from the wind turbine. The reactive stator power reference Q_{ref} is given to get the desired power factor.

SMC allows us to force the stator powers (P_s, Q_s) to track their respective references (P_{ref}, Q_{ref}). In our case, the control law is computed using electric variables referred to as the synchronous reference frame (d, q) We assume that the AC grid voltages $(v_{as}v_{bs}v_{cs})$ and the DFIG stator currents $(i_{as}i_{bs}i_{cs})$ are measured and projected on the (dq) axis to respectively obtain $(v_{ds}v_{qs})$ and $(i_{ds}i_{qs})$. The real components of the DFIG rotor flux $(\varphi_{dr}\varphi_{qr})$ are substituted by their nominal values $(\bar{\varphi}_{dr}\bar{\varphi}_{qr})$. Moreover, the DFIG stator powers (P_s, Q_s) are deduced from measurements of stator currents and voltages. Speed ω_G of the generator shaft is also measured.

The SMC synthesizes the desired rotor voltage sources $(v_{dr}v_{qr})$ corresponding in three-phase form $(v_{ar}v_{br}v_{cr})$, which are used in the PWM block to generate the control impulses in order to drive the AC/AC converter.

2.2. DFIG state space model

In order to control the DFIG, its state space model is carried out in the (d,q) reference frame linked to the vector of stator voltage that is represented by the components $(v_{ds}v_{qs})$. The considered state vector gathers the components of rotor currents $(i_{dr}i_{qr})$, the rotor flux $(\varphi_{dr},\varphi_{qr})$, and the rotor rotating pulsation ω. Moreover, the rotor voltage components $(v_{dr}v_{qr})$ are the vector control. The wind turbine exerts a τ_G torque on the generator shaft, and all frictions on this shaft are taken into account via the τ_{vis} torque.

Therefore, the state vector X and the control vector U are respectively given by:

$$X=(x_1,x_2,x_3,x_4,x_5)^T=(i_{dr},i_{qr},\varphi_{dr},\varphi_{qr},\omega)^T \text{ and } U=(v_{dr},v_{qr})^T.$$

Using our notation, the state model of the DFIG (see Appendix A; on the journal's website) is as given in Eq. (4).

$$\begin{cases} \dot{x}_1=f_1(X)+a_3v_{dr}; \quad f_1=-a_1x_1+\omega_s x_2+a_2x_3-a_3x_5x_4-a_4v_{ds} \\ \dot{x}_2=f_2(X)+a_3v_{qr}; \quad f_2=-\omega_s x_1-a_1x_2+a_2x_4+a_3x_5x_3-a_4v_{qs} \\ \dot{x}_3=f_3(X)+v_{dr}; \quad f_3=-bx_1+\omega_s x_4-x_5x_4 \\ \dot{x}_4=f_4(X)+v_{qr}; \quad f_4=-bx_2-\omega_s x_3+x_5x_3 \\ \dot{x}_5=f_5(X)+c_2(\tau_{vis}+\tau_G); \quad f_5=c_1(x_4x_1-x_3x_2) \end{cases} \tag{4}$$

The positive coefficients of the system in Eq. (4) are given by the following:

$$a_1=\left(\frac{1}{\sigma T_s}+\frac{1}{\sigma T_r}\right) a_2=\frac{1}{\sigma L_r T_s},\ a_3=\frac{1}{\sigma L_r},$$

$$a_4=\frac{(1-\sigma)}{\sigma L_m},\ b=R_r,\ c_1=\frac{P^2}{J},\ c_2=\frac{P}{J},\ \sigma=1-\frac{L_m^2}{L_sL_r}.$$

These coefficients are related to the following machine parameters:

R_r,R_s: rotor and stator resistances.

L_r,L_s,L_m: rotor, stator, and mutual inductances.

P: number of pole pairs.

J : rotor turbine inertia.

T_r,T_s: rotor and stator time constant.

σ: dispersion flux coefficient.

ω_s : stator pulsation.

We assume a perfect orientation of the (q) axis along the stator voltage $(v_{ds}=0)$. Therefore, the active and reactive stator powers of the DFIG are reduced to the following expressions:

$$\begin{cases} P_s=-d_1x_2+d_2x_4 \\ Q_s=-d_1x_1+d_2x_3 \end{cases}, \tag{5}$$

with:

$$d_1=\frac{L_r}{L_m}v_{qs}, d_2=\frac{v_{qs}}{L_m}. \tag{6}$$

2.3. Dynamics of the output

From the DFIG state model, we can derive the following control model:

$$\begin{cases} \dot{Z}=g\left(Z,U\right); \quad Z=\left(P_s,Q_s,x_3,x_4,x_5\right)^T, U=\left(v_{dr},v_{qr}\right)^T \\ Y=h\left(Z\right); \quad Y=\left(P_s,Q_s\right)^T \end{cases} . \tag{7a}$$

Indeed, from Eq. (5), we have:

$$\begin{cases} x_2=\frac{d_2x_4-P_s}{d_1} \\ x_1=\frac{d_2x_3-Q_s}{d_1} \end{cases} . \tag{7b}$$

The derivative times of P_s, Q_s are given by Eq. (7c) as:

$$\begin{cases} \dot{P}_s= -d_1\dot{x}_2+d_2\dot{x}_4 \\ \dot{Q}_s= -d_1\dot{x}_1+d_2\dot{x}_3 \end{cases} . \tag{7c}$$

Using the last equation system, the dynamics of P_s, Q_s are obtained by substituting $\dot{x}_1\dot{x}_2\dot{x}_3\dot{x}_4$ by their expressions given in Eq. (4) and x_1, x_2 by their relations given in Eq. (7b). The dynamics of x_3, x_4, x_5, based on Z, are obtained via replacing x_1, x_2 by their expressions from Eq. (7b) in the three last equations of Eq. (4).

Thus, the state model based on the state vector Z is as follows:

$$\begin{cases} \dot{P}_s= -\xi_1P_s-\omega_sQ_s-\xi_2x_5x_3+\xi_3x_4+\xi_4v_{qs}-\xi_2v_{qr} \\ \dot{Q}_s=\omega_sP_s-\xi_1Q_s+\xi_3x_3+\xi_2x_5x_4+\xi_4v_{ds}-\xi_2v_{dr} \\ \dot{x}_3=\gamma_1Q_s-\gamma_2x_3+(\omega_s-x_5)x_4+v_{dr} \\ \dot{x}_4=\gamma_1P_s-\gamma_2x_4-\left(\omega_s-x_5\right)x_3+v_{qr} \\ \dot{x}_5=\frac{C_1}{d_1}(x_3P_s-x_4Q_s)+c_2\left(\tau_{vis}+\tau_G\right) \end{cases} , \tag{8}$$

where the positive coefficients of the system of Eq. (8) are given by:

$$\xi_1=\frac{1}{\sigma T_s}+\frac{(1-\sigma)}{\sigma T_r}; \quad \xi_2=\frac{(1-\sigma)}{\sigma L_m}v_{qs}; \quad \xi_3=\frac{(1-\sigma)}{\sigma L_mT_r}v_{qs}; \quad \xi_4=\frac{(1-\sigma)L_r}{\sigma L_m^2}v_{qs}; \quad \gamma_1=\frac{L_m}{T_rv_{qs}}; \quad \gamma_2=\frac{1}{T_r}.$$

It is worth noticing that the dynamic model of Eq. (8) is independent of the rotor currents.

2.4. Nominal rotor flux

We intend, in this section, to determine the nominal values $(\bar{\varphi}_{dr}\bar{\varphi}_{qr})$ of the rotor flux components. These values will be used in place of the real value (x_3,x_4) in order to later calculate the proposed control law.

With this target, we consider that the system of Eq. (8) is in a steady-state regime under the nominal stator voltage, and the rotor short circuits without load torque. Under these conditions, Eq. (8) is reduced to:

$$\begin{cases} -\xi_1P_s-\omega_sQ_s-\xi_2x_5x_3+\xi_3x_4+\xi_4v_{qs}= 0 \\ \omega_sP_s-\xi_1Q_s+\xi_3x_3+\xi_2x_5x_4+\xi_4v_{ds}= 0 \\ \gamma_1Q_s-\gamma_2x_3+(\omega_s-x_5)x_4= 0 \\ \gamma_1P_s-\gamma_2x_4-\left(\omega_s-x_5\right)x_3= 0 \\ x_5=\omega_s \end{cases} , \tag{9}$$

which can be rewritten in the following form:

$$\begin{cases} -\xi_2\omega_s x_3+\xi_3 x_4=\xi_1 P_s+\omega_s Q_s-\xi_4 v_{qs} \\ \xi_3 x_3+\xi_2\omega_s x_4=-\omega_s P_s+\xi_1 Q_s \\ \gamma_2 x_3=\gamma_1 Q_s \\ \gamma_2 x_4=\gamma_1 P_s \end{cases}. \tag{10}$$

The powers (P_sQ_s) can be deduced, from the first two equations, as:

$$\begin{pmatrix} P_s \\ Q_s \end{pmatrix}=\begin{pmatrix} \xi_1 & \omega_s \\ -\omega_s & \xi_1 \end{pmatrix}^{-1}\left\{\begin{pmatrix} -\xi_2\omega_s & \xi_3 \\ \xi_3 & \xi_2\omega_s \end{pmatrix}\begin{pmatrix} x_3 \\ x_4 \end{pmatrix}+\begin{pmatrix} \xi_4 v_{qs} \\ 0 \end{pmatrix}\right\}. \tag{11}$$

By replacing (P_s,Q_s), in the two last equations of Eq. (10) by their expressions from Eq. (11), we obtain:

$$\begin{pmatrix} \gamma_2 & 0 \\ 0 & \gamma_2 \end{pmatrix}\begin{pmatrix} x_3 \\ x_4 \end{pmatrix}=\begin{pmatrix} \gamma_1 & 0 \\ 0 & \gamma_1 \end{pmatrix}\begin{pmatrix} \xi_1 & \omega_s \\ -\omega_s & \xi_1 \end{pmatrix}^{-1}\left\{\begin{pmatrix} -\xi_2\omega_s & \xi_3 \\ \xi_3 & \xi_2\omega_s \end{pmatrix}\begin{pmatrix} x_3 \\ x_4 \end{pmatrix}+\begin{pmatrix} \xi_4 v_{qs} \\ 0 \end{pmatrix}\right\} \tag{12}$$

The solution of the system of Eq. (12) related to (x_3,x_4) allows us to determine the nominal rotor flux values as follows:

$$\bar{\varphi}_{dr}=\sqrt{\frac{3}{2}}\frac{(\gamma_{2N}-H_{1N})\gamma_{1N}\xi_{4N}\,|v_s|}{\gamma_{2N}^2-H_{1N}^2-H_{2N}^2},\bar{\varphi}_{qr}=\sqrt{\frac{3}{2}}\frac{-H_{2N}\gamma_{1N}\xi_{4N}\,|v_s|}{\gamma_{2N}^2-H_{1N}^2-H_{2N}^2}, \tag{13}$$

where:

$$H_1=\frac{\omega_s\gamma_1(\xi_1\xi_2+\xi_3)}{\xi_1^2+\omega_s^2},H_2=-\frac{\gamma_1(\xi_1\xi_3-\xi_2\omega_s^2)}{\xi_1^2+\omega_s^2}. \tag{14}$$

$\gamma_{1N},\gamma_{2N},\xi_{4N},H_{1N}$, and H_{2N} stand respectively for $\gamma_1,\gamma_2,\xi_4,H_1$, and H_2 in the case of DFIG nominal parameters.

3. Determination of the sliding mode control

3.1. In ideal case

In this section, based on the DFIG nonlinear state space model of Eq. (8), we intend to develop a SMC of stator powers in order to force the outputs P_s and Q_s tracking their respective references, P_{ref} and Q_{ref}. First, this control law is established in the ideal case (i.e. absence of disturbances and parametric variations).

The sliding surface vector $S=(S_1,S_2)^T$ is taken as the tracking control error of the output vector [20]:

$$\begin{cases} S_1=P_s-P_{ref} \\ S_2=Q_s-Q_{ref} \end{cases}. \tag{15}$$

We assume that P_{ref}, Q_{ref}, and their temporal derivatives $\dot{P}_{ref}$ and $\dot{Q}_{ref}$ are bounded and available. Using Eq. (14), the dynamics of the sliding surface vector S are given by:

$$\begin{cases} \dot{S}_1=\dot{P}_s-\dot{P}_{ref} \\ \dot{S}_2=\dot{Q}_s-\dot{Q}_{ref} \end{cases}, \tag{16}$$

with:

$$\begin{cases} \dot{P}_s - \dot{P}_{ref} = -\xi_1 P_s - \omega_s Q_s - \xi_2 x_5 x_3 + \xi_3 x_4 + \xi_4 v_{qs} - \dot{P}_{ref} - \xi_2 v_{qr} \\ \dot{Q}_s - \dot{Q}_{ref} = \omega_s P_s - \xi_1 Q_s + \xi_3 x_3 + \xi_2 x_5 x_4 + \xi_4 v_{ds} - \dot{Q}_{ref} - \xi_2 v_{dr} \end{cases}. \tag{17}$$

On the other hand:

$$\begin{cases} \dot{S}_1 = -B_1 - \xi_2 v_{qr} \\ \dot{S}_2 = -B_2 - \xi_2 v_{dr} \end{cases}, \tag{18}$$

with:

$$\begin{cases} B_1 = -(-\xi_1 P_s - \omega_s Q_s - \xi_2 x_5 x_3 + \xi_3 x_4 + \xi_4 v_{qs} - \dot{P}_{ref}) \\ B_2 = -\left(\omega_s P_s - \xi_1 Q_s + \xi_3 x_3 + \xi_2 x_5 x_4 + \xi_4 v_{ds} - \dot{Q}_{ref}\right) \end{cases}. \tag{19}$$

We force the dynamics $(\dot{S}_1, \dot{S}_2)$ of the sliding surfaces as follows:

$$\begin{cases} \dot{S}_1 = -k_{s1} sign\,(S_1) - G_{s1} S_1 \\ \dot{S}_2 = -k_{s2} sign\,(S_2) - G_{s2} S_2 \end{cases}, \tag{20}$$

where $k_{s1} k_{s2}, G_{s1}$, and G_{s2} are positive control gains.

Based on the relation of Eq. (18), the condition in Eq. (20) can be fulfilled if the sliding control law is forced as follows:

$$\begin{cases} v_{qr} = \frac{B_1 - k_{s1} sign(S_1) - G_{s1} S_1}{-\xi_2} \\ v_{dr} = \frac{B_2 - k_{s2} sign(S_2) - G_{s2} S_2}{-\xi_2} \end{cases}. \tag{21}$$

At this level, we consider the Lyapunov function:

$$V_c = \frac{1}{2} S^T S. \tag{22}$$

Its time derivative is:

$$\dot{V}_c = \dot{S}^T S. \tag{23}$$

By using Eq. (20), $\dot{V}_c$ is reduced to:

$$\dot{V}_c = -\sum_{i=1}^{2} (k_{si} |S_i| + G_{si} S_i^2). \tag{24}$$

Therefore:

$$\dot{V}_c < 0, \forall S_i \neq 0, \tag{25}$$

which means that the control law of Eq. (21) ensures the convergence of S_i to zero, and the outputs P_s and Q_s track their respective references P_{ref} and Q_{ref}.

3.2. The proposed control law

The proposed control is computed as:

$$\begin{cases} v_{qr} = \frac{B_{10}(\hat{Z}) - k_{s1} sign(S_1) - G_{s1} S_1}{-\xi_{20}} \\ v_{dr} = \frac{B_{20}(\hat{Z}) - k_{s2} sign(S_2) - G_{s2} S_2}{-\xi_{20}} \end{cases}, \tag{26}$$

with:

$$\begin{cases} B_{10}\left(\hat{Z}\right) = -(-\xi_{10}P_s - \omega_s Q_s - \xi_{20}x_5\bar{\varphi}_{dr} + \xi_{30}\bar{\varphi}_{qr} + \xi_{40}v_{qs} - \dot{P}_{sref}) \\ B_{20}\left(\hat{Z}\right) = -\left(\omega_s P_s - \xi_{10}Q_s + \xi_{30}\bar{\varphi}_{dr} + \xi_{20}x_5\bar{\varphi}_{qr} + \xi_{40}v_{ds} - \dot{Q}_{sref}\right) \\ \hat{Z} = (P_s, Q_s, \bar{\varphi}_{dr}, \bar{\varphi}_{qr}, x_5)^T \end{cases} . \tag{27}$$

The elements ξ_{10}, ξ_{20}, ξ_{30}, ξ_{40}, B_{10}, and B_{20} stand respectively for ξ_1, ξ_2, ξ_3, ξ_4, B_1, and B_2 (see Eq. (50)).

We remark from our control law (Eq. (26)) that only the stator currents and voltages are required. Therefore, the rotor current sensor is not used.

3.3. Stability analysis and robustness

In the sequel and under some certain conditions, we establish that the control law (Eq. (26)) is able to ensure the convergence of the sliding surface vector S even in the presence of disturbances (flux estimation errors, modeling errors, parametric variations, and bounded disturbances).

In the real case and under the effects of all disturbances, the terms B_1, B_2, and ξ_2 deviate from their ideal values with ΔB_1,ΔB_2, and $\Delta\xi_2$, respectively. Hence, B_1,B_2, and ξ_2 can be rewritten as follows:

$$\begin{aligned} B_1 &= B_{10}\left(\hat{Z}\right) + \Delta B_1; \quad \Delta B_1 = \varepsilon_{B1} B_{10}\left(\hat{Z}\right), \\ B_2 &= B_{20}\left(\hat{Z}\right) + \Delta B_2; \quad \Delta B_2 = \varepsilon_{B2} B_{20}\left(\hat{Z}\right), \\ \xi_2 &= \xi_{20} + \Delta\xi_2; \quad \Delta\xi_2 = \varepsilon_{\xi_2}\xi_{20}, \end{aligned} \tag{28}$$

where, ε_{B1},ε_{B2}, and ε_{ξ_2} are ratios of deviations.

By using the relations of Eq. (28) and the control law of Eq. (26), the dynamics of sliding surfaces (Eq. (18)) become:

$$\begin{cases} \dot{S}_1 = -(1+\varepsilon_{B1})B_{10} - (1+\varepsilon_{\xi_2})\xi_{20}\frac{B_{10}\left(\hat{Z}\right) - k_{s1}sign(S_1) - G_{s1}S_1}{-\xi_{20}} \\ \dot{S}_2 = -(1+\varepsilon_{B2})B_{20} - (1+\varepsilon_{\xi_2})\xi_{20}\frac{B_{20}\left(\hat{Z}\right) - k_{s2}sign(S_2) - G_{s2}S_2}{-\xi_{20}} \end{cases} . \tag{29}$$

This last relation can be put in the following form:

$$\begin{cases} \dot{S}_1 = (\varepsilon_{\xi_2} - \varepsilon_{B1})B_{10} - (1+\varepsilon_{\xi_2})k_{s1}sign(S_1) - (1+\varepsilon_{\xi_2})G_{s1}S_1 \\ \dot{S}_2 = (\varepsilon_{\xi_2} - \varepsilon_{B2})B_{20} - (1+\varepsilon_{\xi_2})k_{s2}sign(S_2) - (1+\varepsilon_{\xi_2})G_{s2}S_2 \end{cases} . \tag{30}$$

We link to the dynamic of Eq. (30) the Lyapunov function $V_{or} = \frac{1}{2}S^T S$. Its time derivative is given by $\dot{V}_{or} = \dot{S}^T S$. Using Eq. (30), $\dot{V}_{or}$ takes the following form:

$$\begin{aligned} \dot{V}_{or} &= (\varepsilon_{\xi_2} - \varepsilon_{B1})B_{10}\left(\hat{Z}\right)S_1 + (\varepsilon_{\xi_2} - \varepsilon_{B2})B_{20}\left(\hat{Z}\right)S_2 \\ &\quad - (1+\varepsilon_{\xi_2})(k_{s1}|S_1| + k_{s2}|S_2|) - (1+\varepsilon_{\xi_2})(G_{s1}S_1^2 + G_{s2}S_2^2). \end{aligned} \tag{31}$$

We assume that ratios ε_{B1},ε_{B2}, and ε_{ξ_2} are bounded such that $\bar{\varepsilon}_{B1}=max(\,|\varepsilon_{B1}(t)|\,)$, $\bar{\varepsilon}_{B2}=max(\,|\varepsilon_{B2}(t)|\,)$, and $\bar{\varepsilon}_{\xi_2}=\max(\varepsilon_{\xi_2}(t))$; moreover, $\varepsilon_{\xi_2}>0$ (see Appendix B; on the journal's website). Therefore, $\dot{V}_{or}$ fulfills the following inequality:

$$\begin{aligned}\dot{V}_{or} \;\leq\; & (\bar{\varepsilon}_{\xi_2}+\bar{\varepsilon}_{B1})\left|B_{10}\left(\hat{Z}\right)\right||S_1|+(\bar{\varepsilon}_{\xi_2}+\bar{\varepsilon}_{B2})\left|B_{20}\left(\hat{Z}\right)\right||S_2|-(k_{s1}|S_1|+k_{s2}|S_2|)\\ & -(G_{s1}S_1^2+G_{s2}S_2^2).\end{aligned} \tag{32}$$

The control coefficient k_{s1} and k_{s2} are imposed as:

$$k_{s1}\geq(\bar{\varepsilon}_{\xi_2}+\bar{\varepsilon}_{B1})\left|B_{10}\left(\hat{Z}\right)\right|+T_{s1} \text{ and } k_{s2}\geq(\bar{\varepsilon}_{\xi_2}+\bar{\varepsilon}_{B2})\left|B_{20}\left(\hat{Z}\right)\right|+T_{s2} \tag{33}$$

where T_{s1} and T_{s2} are positive constants. Therefore, $\dot{V}_{or}\leq-(G_{s1}S_1^2+G_{s2}S_2^2)<0$, $\forall S_1\neq 0$, and $\forall S_2\neq 0$, which means that $S_i(i=1,2)$ converge asymptotically toward zero. The global stability and robustness of the SMC is then established if the relation from Eq. (33) is verified.

4. Boundedness of DFIG electrical states

In this section, a discussion about the states' boundedness when the DFIG is driven by the proposed low-cost SMC is presented.

4.1. Boundedness of stator powers and their trajectories

Under Eq. (33), it is clear that:

$$k_{s1}\geq T_{s1} \text{ and, } k_{s2}\geq T_{s2} \tag{34}$$

We select two positives constants F_{s1},F_{s2} as follows:

$$\begin{cases} F_{s1}=min\left((1+\varepsilon_{\xi_2})G_{s1}\right) \\ F_{s2}=min\left((1+\varepsilon_{\xi_2})G_{s2}\right)\end{cases}, \tag{35}$$

and so

$$\begin{cases} F_{s1}\leq(1+\varepsilon_{\xi_2})G_{s1} \\ F_{s2}\leq(1+\varepsilon_{\xi_2})G_{s2}\end{cases}. \tag{36}$$

Taking into consideration Eqs. (34), (36), and (30), the sliding regime is involved in such way that:

$$\begin{cases} \dot{S}_i\leq -T_{si}sign(S_i)-F_{si}S_i; & S_i\geq 0 \\ \dot{S}_i\geq -T_{si}sign(S_i)-F_{si}S_i; & S_i\leq 0\end{cases} \quad i=1,2. \tag{37}$$

The system inequality of Eq. (37) implies that:

$$\begin{cases} S_i(t)\leq(S_i(0)+(T_{si}/F_{si}))e^{-F_{si}t}-(T_{si}/F_{si}); & for S_i\geq 0 \\ S_i(t)\geq(S_i(0)-(T_{si}/F_{si}))e^{-F_{si}t}+(T_{si}/F_{si}); & for S_i\leq 0\end{cases}. \tag{38}$$

Using Eq. (38) and starting from $S_i(0)$, the convergence times t_{ci} of $S_i(t)$ to zero are then deduced as:

$$t_{ci}\leq t_{mi} \text{ with } t_{mi}=\frac{1}{F_{si}}ln\left(|S_i(0)|\frac{F_{si}}{T_{si}}+1\right) \text{ and } i=1,2. \tag{39}$$

In the case where the active and reactive stator power references are constants over time intervals greater than $t_{mi}, (i= 1,2)$, the active and reactive powers are bounded and their trajectories are expressed as follows.

$$\begin{cases} P_s(t) \leq ((P_s(0) - P_{ref}) + (T_{si}/F_{si}))\, e^{-F_{s1}t} - (T_{s1}/F_{s1}) + P_{ref}; & P_s(0) \geq P_{ref}; \quad t \leq t_{c1} \\ P_s(t) \geq ((P_s(0) - P_{ref}) - (T_{si}/F_{si}))\, e^{-F_{s1}t} + (T_{s1}/F_{s1}) + P_{ref}; & P_s(0) \leq P_{ref}; \quad t \leq t_{c1} \\ P_s(t) = P_{ref}; \quad t \geq t_{c1} \end{cases} \tag{40}$$

$$\begin{cases} Q_s(t) \leq ((Q_s(0) - Q_{ref}) + (T_{si}/F_{si}))\, e^{-F_{s2}t} - (T_{s2}/F_{s2}) + Q_{ref}; & Q_s(0) \geq Q_{ref}; \quad t \leq t_{c2} \\ Q_s(t) \geq ((Q_s(0) - Q_{ref}) - (T_{si}/F_{si}))\, e^{-F_{s2}t} + (T_{s2}/F_{s2}) + Q_{ref}; & Q_s(0) \leq Q_{ref}; \quad t \leq t_{c2} \\ Q_s(t) = Q_{ref}; \quad t \geq t_{c2} \end{cases} \tag{41}$$

4.2. Boundedness and trajectories of rotor flux components

In this subsection, we find the evolution of the (dq) components of the rotor flux while our low-cost SMC is applied.

Recall that in the (dq) reference frame, the usual DFIG model is given by the following equations:

$$\begin{cases} v_{ds} = R_s i_{ds} + \frac{d\varphi_{ds}}{dt} - \omega_s \varphi_{qs} \\ v_{qs} = R_s i_{qs} + \frac{d\varphi_{qs}}{dt} + \omega_s \varphi_{ds} \\ v_{dr} = R_r i_{dr} + \frac{d\varphi_{dr}}{dt} - (\omega_s - \omega)\varphi_{qr} \\ v_{qr} = R_r i_{qr} + \frac{d\varphi_{qr}}{dt} + (\omega_s - \omega)\varphi_{dr} \end{cases} \tag{42}$$

and

$$\begin{cases} \varphi_{ds} = L_s i_{ds} + L_m i_{dr} \\ \varphi_{qs} = L_s i_{qs} + L_m i_{qr} \\ \varphi_{dr} = L_r i_{dr} + L_m i_{ds} \\ \varphi_{qr} = L_r i_{qr} + L_m i_{qs} \end{cases}. \tag{43}$$

From Eq. (43), we have the expression of the rotor flux components as follows:

$$\begin{pmatrix} \varphi_{dr} \\ \varphi_{qr} \end{pmatrix} = \frac{L_r}{L_m} \begin{pmatrix} \varphi_{ds} \\ \varphi_{qs} \end{pmatrix} - \sigma \frac{L_s L_r}{L_m} \begin{pmatrix} i_{ds} \\ i_{qs} \end{pmatrix}. \tag{44}$$

By neglecting the terms $R_s i_{ds}$ and $R_s i_{qs}$ in two first equations of Eq. (42), we obtain:

$$\begin{cases} v_{ds} \cong \frac{d\varphi_{ds}}{dt} - \omega_s \varphi_{qs} \\ v_{qs} \cong \frac{d\varphi_{qs}}{dt} + \omega_s \varphi_{ds} \end{cases}. \tag{45}$$

By assuming that the (q) axis is linked to the voltage vector ($v_{ds} = 0$), the stator flux components are approximated by:

$$\begin{cases} \varphi_{ds} \cong \frac{v_{qs}}{\omega_s} \\ \varphi_{qs} \cong 0 \end{cases}. \tag{46}$$

Using expressions of the nominal rotor flux components from Eq. (12) and taking into account DFIG parameters values as given in the Table, we obtain:

$$\begin{cases} \varphi_{ds} \cong \bar{\varphi}_{dr} \\ \varphi_{qs} \cong \bar{\varphi}_{qr} \end{cases}, \tag{47}$$

and Eq. (44) becomes:

$$\begin{pmatrix} \varphi_{dr} \\ \varphi_{qr} \end{pmatrix} = \frac{L_r}{L_m} \begin{pmatrix} \bar{\varphi}_{dr} \\ \bar{\varphi}_{qr} \end{pmatrix} - \sigma \frac{L_s L_r}{L_m} \begin{pmatrix} i_{ds} \\ i_{qs} \end{pmatrix}. \tag{48}$$

Taking into account the magnitude order of the DFIG parameters ($\frac{L_r}{L_m} \cong 1, \sigma \frac{L_s L_r}{L_m} \ll 0.001$), the relations of Eq. (48) confirm well that the rotor flux components values evolve around their nominal values. Therefore, the boundedness of the flux in transient and steady-state regime is confirmed.

Table. Wind turbine chain parameters.

Symbol	Quantity	Numerical value
P_N	DFIG nominal power	1.5 MW
$P\ f_s\ R_{sN}$	Pole pairs number	2
	Grid frequency	50 Hz
	Nominal stator resistance	0.012Ω
R_{rN}	Nominal rotor resistance	0.021Ω
L_{sN}	Nominal stator inductance	$0.0137H$
L_{rN}	Nominal rotor inductance	$0.0137H$
L_{mN}	Nominal mutual inductance	$0.0135H$
f	Viscosity coefficient	7.110^{-3}
J	Inertia	$50kgm^2$
$FreN$	Nominal grid frequency	50 Hz
$\|v_s\|$	Nominal grid voltage amplitude	$690\sqrt{2}$ V
Pal	Pole number	3
R	Pole diameter	35.5 m
C_p	Turbine characteristic	$0.5 \sin(\pi(\lambda+0.1)/18.2)$
β	Orientation angle	0
m_c	Multiplier gain	65
$G_{si}k_{si}$ ($\bar{\varphi}_{dr}\bar{\varphi}_{qr}$)	SMC gains Nominal rotor flux	10^5,10^4 (3.8, 0) Web

4.3. Boundedness of rotor current

Since the stator powers and rotor flux components are bounded, and based on Eq. (5), the rotor currents components can be bounded as follows:

$$\begin{cases} |x_1| \leq \left|\frac{1}{d_1}\right| Max\left(|Q_s(0)|, |Q_{ref}|\right) + \left|\frac{d_2}{d_1}\right| |x_3| \\ |x_2| \leq \left|\frac{1}{d_1}\right| Max\left(|P_s(0)|, |P_{ref}|\right) + \left|\frac{d_2}{d_1}\right| |x_4| \end{cases}. \tag{49}$$

Consequently, in Section 4, we have proved the boundedness of the DFIG electrical states, such as the stator powers, rotor flux, and current components, when our control law is applied. The boundedness is well established in the transient and steady-state regime.

5. Simulation results

The simulations of the considered WECS, as shown in Figure 1, are carried out in the case of a DFIG rated at 1.5 MW. Its parameters and those related to the AC grid, the wind turbine, and our low-cost SMC are given in the Table. We assume that the WECS operates beyond the starting step. The lumped inertia constant of the system is set to a relatively small value of 50 kg m ^{2} in this study to reduce the simulation time.

5.1. Comparative study

In order to evaluate the SMC performances, two simulations are carried out. The first simulation (SMC-I) concerns the computation of the SMC using Eq. (21) in the ideal case, where the real rotor flux values ($x_3 x_4$) and DFIG parameters are assumed to be available. The case of an unbalanced grid is not considered. The second simulation (SMC-II) is carried out in the case where the SMC is computed using Eq. (26), and all DFIG parameters are supposed to not be well known.

In order to evaluate the performances of the proposed SMC-II, it is sufficient to compare its results with those of SMC-I. The control law of SMC-II is tested in the presence of perturbations (parametric variations related to $\Delta R_s = +25\%$, $\Delta R_r = +50\%$, $\Delta L_s = -50\%$, $\Delta L_r = -50\%$, and $\Delta L_m = -50$) and also an unbalanced voltage grid (Figure 2a). The simulation results related to SMC-II and SMC-I are shown in the Figures 2b and 2c, respectively. From these results, it appears that the active and reactive powers track their references with acceptable error bounds. The stator and rotor currents remain in acceptable limits for this rated machine.

These results reveal that the responses of the DFIG driven respectively by SMC-II and SMC-I are basically the same. These results highlight the good robustness of the proposed control law.

5.2. Response to MPPT

We assume that the wind turbine is moved by the wind with the speed (V_w) profile given in Figure 3a. The low-cost SMC is computed using the control law of Eq. (26). The parametric variations and an unbalanced voltage grid are applied in the time interval of $[100s,\ 150s]$. We consider the variation of voltage frequency with +5% and the variation of voltage phase modulus with +20%. The parametric variations are represented by the variation of all resistances with +50% and by the variation of all inductances with –50%.

The wind turbine operates near the optimal speed necessary to extract the maximum wind power (Figure 3b). This is confirmed by the evolution of the power coefficient, which sensibly remains at its maximum value (Figure 3c) since the active stator power follows its reference (Figure 3d) and the reactive stator power varies within a weak bound around its reference (Figure 3e). Furthermore, the rotor currents and flux remain in acceptable limits for this rated generator (Figures 3f and 3g), so we can deduce that this wind turbine is well adapted to the DFIG operation for this wind speed regime. As we have demonstrated above, the rotor flux components remain near their nominal values.

6. Conclusion

In this paper, we have developed a sliding mode control of the powers provided by a WECS incorporating a DFIG without using any estimation model of rotor flux or any rotor current sensor. The proposed control law can be qualified as low-cost SMC. Indeed, the synthesis of the controller is carried out based on the nonlinear and coupled DFIG model. On one hand, we have established the global stability of the control law even in the presence of disturbances affecting the plant model (i.e. parametric variations, flux estimation error, modeling

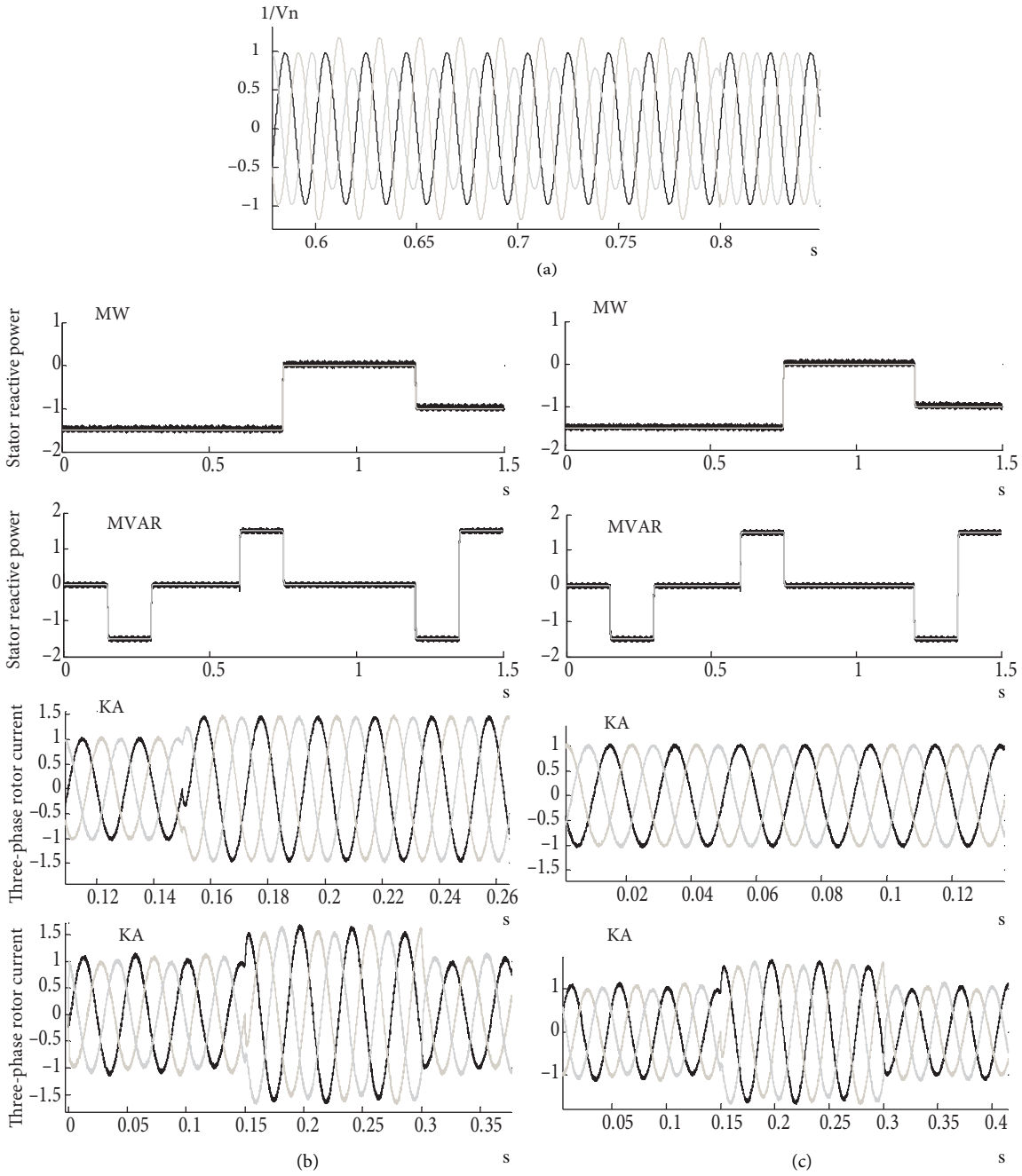

Figure 2. Simulation results: (a) the unbalanced voltage of the grid, $V_n = |v_s|$; (b) SMC-II; (c) SMC-I.

errors, and unbalanced voltage grid). On the other hand, we have verified the boundedness of the electrical states when the proposed control law drives the plant. It is proved that the components of the rotor flux remain near their nominal values when our low-cost SMC is applied. Our low-cost SMC is developed based on this latter point, the robustness of the SMC, and the DFIG state model, which contain as states only the stator powers, the rotor flux components, and rotating pulsation. Rotor current components are not used (thus, no rotor current sensor is used).

The simulation tests of the proposed method are achieved in the case of a WECS based on a DFIG

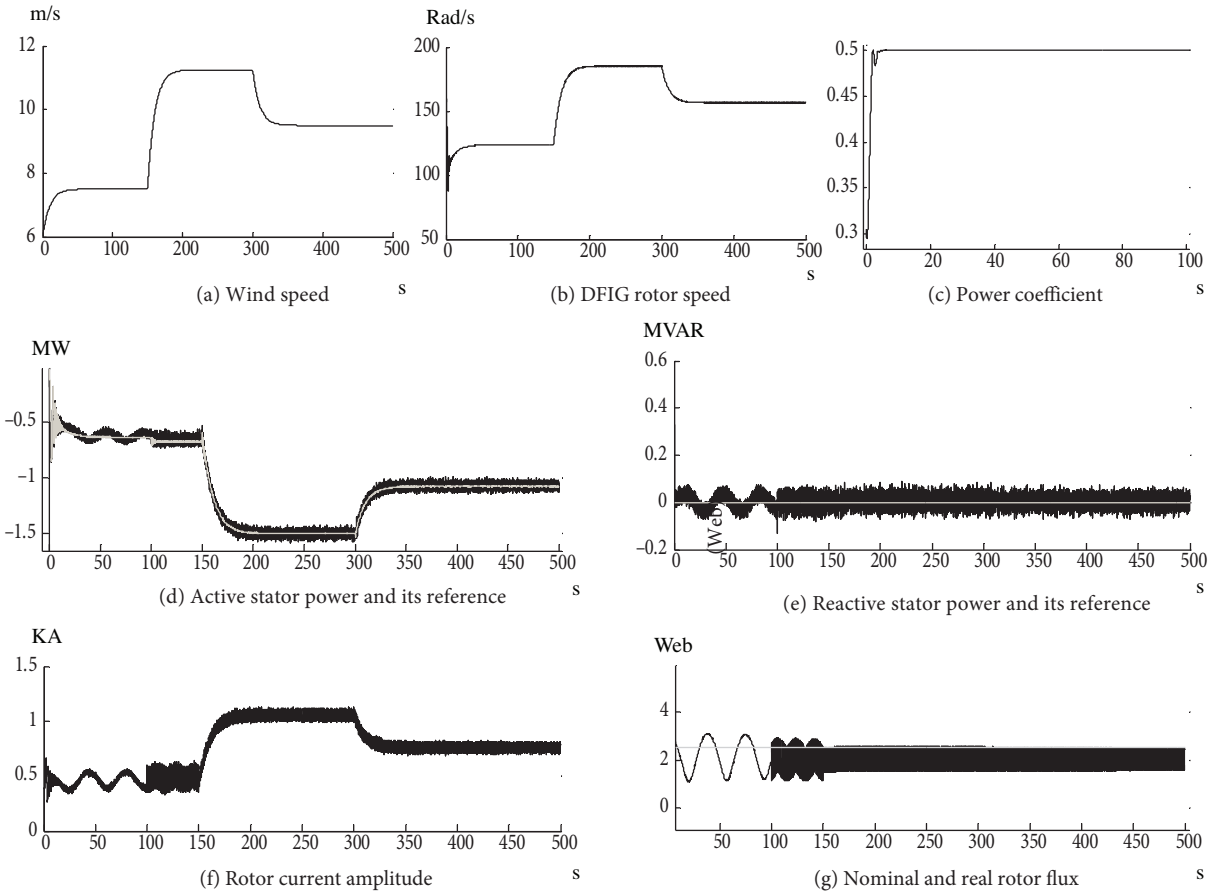

Figure 3. Wind chain simulation results.

rated at 1.5 MW. The obtained results confirm that the proposed control law keeps the same robustness and performances compared to SMC with real rotor flux and known parameters, and it is feasible with the MPPT algorithm.

Note: the DFIG parameters taken in the calculation of the control law of Eq. (26) are:

$$(R_{s0}, R_{r0}, L_{s0}, L_{r0}, L_{m0}) = (R_{sN}, R_{rN}, 2L_{sN}, 2L_{rN}, 2L_{mN})\,. \tag{50}$$

References

[1] EurObserv'ER. Wind power barometer. Le Journal de l'Eolien 2012; 10: 80–107.

[2] Mohammadi J, Vaez-Zadeh S, Afsharnia S, Daryabeigi E. A combined vector and direct power control for DFIG-based wind turbines. IEEE T Sustain Energ 2014; 5: 767–775.

[3] Shuhui L, Haskew TA, Williams KA, Swatloski RP. Control of DFIG wind turbine with direct-current vector control configuration. IEEE T Sustain Energ 2012; 3: 1–11.

[4] Liyan Q, Wei Q. Constant power control of DFIG wind turbines with super capacitor energy storage. IEEE T Ind Appl 2011; 47: 359–367.

[5] Belmokhtar K, Doumbia ML, Agbossou K. Novel fuzzy logic based sensor-less maximum power point tracking strategy for wind turbine systems driven DFIG (doubly-fed induction generator). Energy 2014; 76: 679–693.

[6] Beltran B, Benbouzid MEH, Ahmed-Ali T. Second-order sliding mode control of a doubly fed induction generator driven wind turbine. IEEE T Energy Conver 2012; 27: 261–269.

[7] Yu Z, Elbuluk ME. Stability analysis of maximum power point tracking (MPPT) method in wind power systems. IEEE T Ind Appl 2013; 49: 1129–1136.

[8] Jiabing H, Yikang H, Lie X. Improved rotor current control of wind turbine driven doubly-fed induction generators during network voltage unbalance. Electr Pow Syst Res 2010; 80: 847–856.

[9] Chen SZ, Cheung NC, Wong KC, Wu J. Integral variable structure direct torque control of doubly fed induction generator. IET Renew Power Gen 2011; 5: 18–25.

[10] Chen SZ, Cheung NC, Wong KC, Wu J. Integral sliding-mode direct torque control of doubly-fed induction generators under unbalanced grid voltage. IEEE T Energy Conver 2010; 25: 356–368.

[11] Martinez MI, Tapia G, Susperregui A, Camblong H. Sliding-mode control for DFIG rotor- and grid-side converters under unbalanced and harmonically distorted grid voltage. IEEE T Energy Conver 2012; 27: 328–339.

[12] Hua G, Cong L, Geng Y. LVRT capability of DFIG-based WECS under asymmetrical grid fault condition. IEEE T Ind Electron 2013; 60: 2495–2509.

[13] Nian H, Cheng P, Zhu ZQ. Independent operation of DFIG-based WECS using resonant feedback compensators under unbalanced grid voltage conditions. IEEE T Power Electr 2014; 99: 1–12.

[14] Rezaei E, Tabesh A, Ebrahimi M. Dynamic model and control of DFIG wind energy systems based on power transfer matrix. IEEE T Power Deliver 2012; 27: 1485–1493.

[15] Hu J, Nian H, Hu B, He Y, Zhu ZQ. Direct active and reactive power regulation of DFIG using sliding-mode control approach. IEEE T Energy Conver 2010; 25: 1028–1039.

[16] Abad G, Rodriguez MA, Poza J. Two-level VSC-based predictive direct power control of the doubly fed induction machine with reduced power ripple at low constant switching frequency. IEEE T Energy Conver 2008; 23: 570–580.

[17] Abad G, Rodriguez MA, Poza J. Two-level VSC-based predictive torque control of the doubly fed induction machine with reduced torque and flux ripples at low constant switching frequency. IEEE T Power Electr 2008; 23: 1050–1061.

[18] Susperregui A, Martinez MI, Zubia I, Tapia G. Design and tuning of fixed-switching-frequency second-order sliding-mode controller for doubly fed induction generator power control. IET Electr Power Appl 2012; 6: 696–706.

[19] Evangelista C, Puleston P, Valenciaga F, Fridman LM. Lyapunov-designed super-twisting sliding mode control for wind energy conversion optimization. IEEE T Ind Electron 2013; 60: 538–548.

[20] Slotin JJE. Sliding controller design for non-linear systems. Int J Control 1984; 43: 421–434.

A. Appendix

Recall that $\xi_2=\frac{(1-\sigma)}{\sigma L_m}v_{qs}$, and it takes the value of $\xi_{20}=\frac{(1-\sigma_0)}{\sigma_0 L_{m0}}v_{qs}$ under Eq. (50),

Where σ_0 stand for σ under Eq. (50).

The DFIG mutual stator and rotor inductances vary practically, both with same percentage. This implies that $\sigma=\sigma_0, \xi_{20}=\frac{(1-\sigma)}{\sigma L_{m0}}v_{qs}$, and $\Delta\xi_2=\frac{(1-\sigma)}{\sigma}\left(\frac{1}{L_m}-\frac{1}{L_{m0}}\right)$.

The deviation ratio is $\varepsilon_{\xi_2}=\frac{\Delta\xi_2}{\xi_{20}}=\frac{L_{m0}}{L_m}-1$.

If we impose a value of L_{m0} in such way that $L_m<L_{m0}$, we obtain $\varepsilon_{\xi_2}>0$.

B. Appendix

In this appendix, we expose the demarche used to find the state model of Eq. (4) as its matrix form.

From Eq. (42), we obtain:

$$\begin{cases} \frac{d\varphi_{ds}}{dt}=v_{ds}-R_s i_{ds}+\omega_s\varphi_{qs} \\ \frac{d\varphi_{qs}}{dt}=v_{qs}-R_s i_{qs}-\omega_s\varphi_{ds} \\ \frac{d\varphi_{dr}}{dt}=v_{dr}-R_r i_{dr}+(\omega_s-\omega)\varphi_{qr} \\ \frac{d\varphi_{qr}}{dt}=v_{qr}-R_r i_{qr}-(\omega_s-\omega)\varphi_{dr} \end{cases}. \tag{B.1}$$

We rewrite the equation system of Eq. (43) as:

$$\begin{cases} i_{ds}=\frac{1}{L_m}\varphi_{dr}-\frac{L_r}{L_m}i_{dr} \\ i_{qs}=\frac{1}{L_m}\varphi_{qr}-\frac{L_r}{L_m}i_{qr} \\ \varphi_{ds}=\frac{L_s}{L_m}\varphi_{dr}-\frac{\sigma}{1-\sigma}L_m i_{dr} \\ \varphi_{qs}=\frac{L_s}{L_m}\varphi_{qr}-\frac{\sigma}{1-\sigma}L_m i_{qr}; \quad \sigma=1-\frac{L_m^2}{L_s L_r} \end{cases}. \tag{B.2}$$

Substituting Eq. (B.2) into Eq. (B.1), we get:

$$\begin{cases} \frac{L_s}{L_m}\frac{d\varphi_{dr}}{dt}-\frac{\sigma}{1-\sigma}L_m\frac{di_{dr}}{dt}=v_{ds}-R_s\left(\frac{1}{L_m}\varphi_{dr}-\frac{L_r}{L_m}i_{dr}\right)+\omega_s\left(\frac{L_s}{L_m}\varphi_{qr}-\frac{\sigma}{1-\sigma}L_m i_{qr}\right) \\ \frac{L_s}{L_m}\frac{d\varphi_{qr}}{dt}-\frac{\sigma}{1-\sigma}L_m\frac{di_{qr}}{dt}=v_{qs}-R_s\left(\frac{1}{L_m}\varphi_{qr}-\frac{L_r}{L_m}i_{qr}\right)-\omega_s\left(\frac{L_s}{L_m}\varphi_{dr}-\frac{\sigma}{1-\sigma}L_m i_{dr}\right) \\ \frac{d\varphi_{dr}}{dt}=v_{dr}-R_r i_{dr}+(\omega_s-\omega)\varphi_{qr} \\ \frac{d\varphi_{qr}}{dt}=v_{qr}-R_r i_{qr}-(\omega_s-\omega)\varphi_{dr} \end{cases}. \tag{B.3}$$

In the last system, if we substitute the two last equations in the two first equations, we obtain the DFIG state

model of Eq. (B.4), based on $i_{dr}, i_{qr}, \varphi_{dr}\varphi_{qr}, \omega$, as:

$$\begin{cases} \frac{di_{dr}}{dt}=-a_1 i_{dr}+\omega_s i_{qr}+a_2\varphi_{dr}-a_3\omega\varphi_{qr}-a_4 v_{ds}+a_3 v_{dr} \\ \frac{di_{qr}}{dt}= -\omega_s i_{dr}-a_1 i_{qr}+a_2\varphi_{qr}+a_3\omega\varphi_{dr}-a_4 v_{qs}+a_3 v_{qr} \\ \frac{d\varphi_{dr}}{dt}= -bi_{dr}+\omega_s\varphi_{qr}-\omega\varphi_{qr}+v_{dr} \\ \frac{d\varphi_{qr}}{dt}= -bi_{qr}-\omega_s\varphi_{dr}+\omega\varphi_{dr}+v_{qr} \\ \frac{d\omega}{dt}=c_1\left(\varphi_{qr}i_{dr}-\varphi_{dr}i_{qr}\right)+c_2\left(\tau_{vis}+\tau_G\right) \end{cases} . \tag{B.4}$$

The coefficients of Eq. (B.4) are given by:

$$a_1=\left(\frac{1}{\sigma T_s}+\frac{1}{\sigma T_r}\right) a_2=\frac{1}{\sigma L_r T_s}, a_3=\frac{1}{\sigma L_r}, a_4=\frac{(1-\sigma)}{\sigma L_m}, b=R_r, c_1=\frac{P^2}{J}, c_2=\frac{P}{J}.$$

The state model of Eq. (B.4) can be rewritten another way, in the form of a matrix, as:

$$\begin{cases} \frac{d}{dt}\begin{pmatrix} i_{dr} \\ i_{qr} \\ \varphi_{dr} \\ \varphi_{qr} \end{pmatrix} = \begin{pmatrix} -a_1 & \omega_s & a_2 & -a_3\omega \\ -\omega_s & -a_1 & a_3\omega & a_2 \\ -b & 0 & 0 & (\omega_s-\omega) \\ 0 & -b & -(\omega_s-\omega) & 0 \end{pmatrix} \begin{pmatrix} i_{dr} \\ i_{qr} \\ \varphi_{dr} \\ \varphi_{qr} \end{pmatrix} + \begin{pmatrix} -a_4 v_{ds}+a_3 v_{dr} \\ -a_4 v_{qs}+a_3 v_{qr} \\ v_{dr} \\ v_{qr} \end{pmatrix} \\ \frac{d\omega}{dt}=c_1\left(\varphi_{qr}i_{dr}-\varphi_{dr}i_{qr}\right)+c_2\left(\tau_{vis}+\tau_G\right) \end{cases} . \tag{B.5}$$